Energy & Environmental Science

Versatile Single-Ion Electrolyte with Grotthuss-like Li Conduction Mechanism for Dendrite-Free Li Metal Batteries

Journal:	*Energy & Environmental Science*
Manuscript ID	EE-ART-05-2019-001473.R1
Article Type:	Paper
Date Submitted by the Author:	28-Jun-2019
Complete List of Authors:	Yuan, Shouyi; Fudan University, Department of Chemistry Bao, Junwei; University of Minnesota, Chemistry Wei, Ji-Shi; Fudan University, Xia, Yong-Yao; Institute of New Energy, Department of Chemistry Truhlar, Donald; Department of Chemistry, University of Minnesota Wang, Yonggang; Fudan University, Department of Chemistry; National Institute of Advanced Industrial Science and Technology (AIST), Energy Technology Research Institute

ARTICLE

Versatile Single-Ion Electrolyte with Grotthuss-like Li Conduction Mechanism for Dendrite-Free Li Metal Batteries

Received 00th January 20xx,
Accepted 00th January 20xx

DOI: 10.1039/x0xx00000x

Shouyi Yuan[a], Junwei Lucas Bao[b], Jishi Wei[a], Yongyao Xia[a], Donald G. Truhlar[b]* and Yonggang Wang[a]*

Abstract: Batteries with Li metal anodes have the desirable feature of high energy density; however, the notorious problem of Li dendrite formation has impeded their practical applications. Herein, we present a versatile single-ion electrolyte, which is achieved by a different strategy of coordinating the anions in the electrolyte on the open metal sites of metal organic framework. Further investigations of the activation energy and theoretical quantum mechanical calculation suggest that Li ion transport inside the pore of the Cu-MOF-74 is via a Grotthuss-like mechanism that the charge is transported by coordinated hopping of Li ion between the perchlorate groups. This single-ion electrolyte is versatile, which has wide applications. When the single-ion electrolyte is used for Li||Li symmetric cells and Li||$LiFePO_4$ full cells, the Li dendrites is suppressed. As a result, ultralong cycle lives are achieved for both cells. In addition, when the single-ion electrolyte is assembled into the Li||$LiMn_2O_4$ batteries, the dissolution of Mn^{2+} into the electrolyte is suppressed even at elevated temperature, and a long cycle life with improved capacity retention is achieved for Li||$LiMn_2O_4$ batteries. Finally, when the single-ion electrolyte is applied to Li-O_2 batteries, an improved cycle life with reduced overpotential is also achieved.

Introduction

With the rapid popularization of electric vehicles, there is an urgent demand for batteries with high energy density and high specific capacity such as Li-sulfur batteries and Li-air batteries.[1] Li metal anodes would be especially suitable for this kind of application because of their high specific capacity (3860 mAh g^{-1}), which is far beyond that of commercial graphite anodes (372 mAh g^{-1}).[2-4] However, although there has been steady progress improving the cathode side of Li-air batteries and Li sulfur batteries[5-10], the use of Li metal anodes still suffers from irregular deposition of Li ions on the anode, and the resulting formation of Li dendrites that causes internal short circuits, which will lead to hazardous explosions. The Li dendrites also lead to capacity loss due to depletion of Li from the anode.[2-4] Therefore, it is critical to address the issue of Li dendrite formation.

Various strategies have been put forward to address the issue of Li dendrites, inclduing optimizing the electrolyte[11-18], engineering artificial solid electrolyte interfaces[19-23], and designing structured anodes[24-32]. However, although those strategies effectively prolong the cycle life of Li-metal batteries, they do not solve the intrinsic instability of Li metal in liquid-electrolyte batteries. Hence, the Li dendrites still form in the long term.

It is widely acknowledged that the conventional liquid electrolyte for Li-metal batteries contains the lithium salts and organic solvents, such as 1M $LiPF_6$ in ethylene carbonate/diethyl carbonate(EC/DEC). During charge/discharge, both cations (e.g. Li^+) and anions (e.g. PF_6^-) in electroltye move towards the opposite direction along with the electron transfer between cathode and anode. The mobility of the anions actively contributes to the ion conduction process in batteries, but they do not participate in the electrode reactions. Thus, during the Li stripping process, the electrical field drives the anions in the electrolyte towards the anodic side, where they gradually accumulate near the anode. This causes concentration polarization, which may lead to the formation of an ion depletion layer.[33, 34] Previous reports[33,34] have shown that tiny and random lithium deposition takes place at the ion depletion layer on the surface of lithium metal, triggering the growth of Li dendrites. Therefore, immobilzing the anions in the electrolyte would be an efficient solution for Li dendrite in the electrolyte.

Inorganic solid-state electrolytes are the ultimate solution for Li dendrites, because they fundamentally change the behavior of Li deposition.[35-37] Inorganic solid-state electrolytes have the advantage of being single-ion conductors that can have a high Li-ion transference number close to 1 and negligible electronic conductivity. Theoretical studies have also demonstrated that the utilization of active materials may remain close to 100% even at relatively high charge/discharge current with single-ion electrolyte.[33,34,38] In addition, Li dendrite growth in the

[a] *Department of Chemistry, Shanghai Key Laboratory of Catalysis and Innovative Materials, Center of Chemistry for Energy Materials, Fudan University, Shanghai, 200433, China.* ***E-mail:*** *ygwang@fudan.edu.cn*
[b] *Department of Chemistry, Chemical Theory Center, and Minnesota Supercomputing Institute, University of Minnesota, 207 Pleasant Street SE, Minneapolis, Minnesota 55455-0431, USA.* ***E-mail:*** *truhlar@umn.edu*
Electronic Supplementary Information (ESI) available: [details of any supplementary information available should be included here]. See DOI: 10.1039/x0xx00000x

electrolyte has been investigated, where they show that Li dendrite growth is suppressed when the anions in the electrolyte are partially immobilized.[39-41] As a result, the single-ion electrolyte has been demonstrated excellent capability to suppress the Li dendrites.[34,42] Countering these advantages though are new challenges arising from the interfacial contact between electrode (especially the cathode side) and inorganic solid-state electrolyte[36]. Another traditional approach to realize single-ion transport in the elecrtrolyte is to employ polymer as the electrolyte backbone with some strategies to immobilize the anions including covalently linking the anions to the polymeric backbone, attaching anions to the inorganic backbone, and addition of trapping agents for anions to dual-ion conducting SPEs.[33] Nevertheless, the ion conductivity of the single-ion polymer electrolyte is inferior especially at room temperature.[33] Despite the rapid development made in the solid-state batteries, major obstacles still remain for the commercialization of all solid-state batteries. Hence, we are motivated to realize single-ion transport in the liquid electrolyte. Zhou *et al.*[42] previously demonstrated that the single-ion transport in the batteries can be obtained with a MOF memberane infiltrated with electrolyte. However, since the anions in their paper have no interreaction with MOF matrix, they can also cross the membrane through the interparticle voids between MOF particles.

Herein, we show that another possible kind of single-ion conductor in the liquid electrolyte can be prepared by coordinating the anions (in particular ClO_4^-) in the liquid electrolyte on the open metal sites of a metal organic framework (MOF) matrix as a way to bring about homogeneous single Li-ion transport in the electrolyte. Further investigations of the activation energy and theoretical calculations suggest that the solvated Li^+ outside the MOF pores is preferentially adsorbed into the pore of the MOF due to abundant lithiophilic and electronegative ClO_4^- inside the the pore MOF, and the Li^+ ions migrate within the pores of the MOF by a Grotthuss-like mechanism involving hopping of solvated Li^+ between ClO_4^- groups. Thus, the Li ion transport in the single-ion electrolyte is dominated by this transport within the pores of the MOF.

The single-ion electrolyte presented here is versatile and has a wide range of application. When it is used in Li||Li symmetric batteries, the Li dendrites are effectively suppressed, and an ultralong cycle life over 2000 h with low voltage hysteresis is obtained. When the single-ion electrolyte is used in Li||$LiFePO_4$ full cells, we achieve a long cycle life over 2000 cycles. Furthermore, when the single-ion electrolyte is assembled into Li||$LiMn_2O_4$ batteries, it can effectively suppress the dissolution of Mn^{2+}, and thus the cycling stability of the Li||$LiMn_2O_4$ full cells is improved even at elevated temperature. Finally, when the single-ion electrolyte is used for a Li-O_2 battery, we can achieve improved cycle stability with reduced overpotential.

Experimental Section

Preparation of the Single-ion Electrolyte

Cu-MOF-74 was synthesized via a hydrothermal method. In particular, $Cu(NO_3)_2$ (0.966g, 4mmol) and 2,5-dihydroxyterephthalic acid (0.396g, 2mmol) were dissolved into the mixture solvent of N,N-Dimethyformamide and ethanol in a ratio of 20:1 (40ml). Then, the solution was transferred into the autoclave and hydrothermal-treated at 80 °C for 20 h. After that, the precipitates were washed by ethanol for several times and then collected by centrifugation. Subsequently, the precipitates were immersed into the hot ethanol at 70 *°C* for 7 days. Finally, the precipitates were dried at 120 °C under vacuum overnight and further activated at 200 °C under vacuum overnight.

To prepare the single-ion electrolyte pellets, the as-synthesized Cu-MOF-74 powder was mixed with PTFE in a ratio of 9:1 and pressed into a pellet. The pellets were further compacted under 20 tons of pressure to remove the interparticle pores. Eventually, the pellets were immersed into the 1M $LiClO_4$ DOL/DME electrolyte for Li||Li symmetric batteries, 1M $LiClO_4$ PC electrolyte for $LiFePO_4$-Li full cells and 1M $LiClO_4$ TEGDME for Li-O_2 batteries at 80°C overnight. Then, the pellets were taken out, wiped out with tissues and dried under vacuum for 2 hours.

Materials Characterization:

The morphologies of all the materials were investigated by the Scanning Electronic Microscopic (SEM) (FE-SEM S-4800) and Transmission Electron Microscope (TEM) (JEOL JEM-2100 F microscope (Japan) operated at 200 kV). The Energy Dispersive Spectrometer (EDS) mapping was carried out, which is equipped in the SEM; Scanning transmission electron microscopy (STEM) mapping was carried out, which is equipped in TEM. X-ray photoelectron spectroscopy (XPS) was carried out on aXSAM800 Ultra spectrometer. Powder X-ray diffraction was carried out on a X-ray diffractometer (Bruker D8 Advance, Germany) with Cu Kα radiation (λ = 0.15406 nm). The specific surface area is investigated by Brunauer-Emmett-Teller (BET) method. The samples for BET measurement were degassed at 150 °C under vacuums overnight.

Electrochemical measurement

The ion conductivity was measured by electrochemical impedance spectroscopy (EIS) by sandwiching the electrolyte between two stainless steel. The EIS spectrum was carried out on an AUTOLAB electrochemical work station (PGSTAT 302N) from 1MHz to 1 Hz. Electrochemical window of the single-ion electrolyte was measured by cyclic voltammetry with a scan rate of 1mV S^{-1}

The $LiFePO_4$ cathodes were prepared by grinding the commercialized $LiFePO_4$ powder with Super P and PVDF powder in a ratio of 7:2:1. Subsequently, the mixture was stirred in the NMP solvent and slurried on the aluminum foil. Finally, the cathode was dried under vacuum at 80 *°C* overnight. The $LiMn_2O_4$ cathode was also prepared by the same way. The average cathode loading is about 3.0 mg cm^{-2} based on the weight of active materials.

To assemble the $LiFePO_4$ full cells, Li metals were employed as the counterpart electrode. Then, the cells were assembled by

sandwiching the single-ion electrolyte between $LiFePO_4$ cathode and Li metal anode. For comparison, the Li||$LiFePO_4$ full cells were also prepared with Celgard 2300 dipping with 1M $LiClO_4$ PC electrolyte. The Li||$LiMn_2O_4$ full cells were also assembled by the same way.

To prepare the Li-O_2 cells, the cathode was prepared by mixing Kejenblack with PVdF in a ratio of 9:1. Then, the mixture was slurried on the carbon papers, which were dried under 120 ^oC overnight. The average cathode loading is 0.5 mg cm^{-2} (based on the weight of Kejenblack).

The Li-O_2 batteries were assembled with CR2036 Li-O_2 coin cell in the glovebox filled with Ar. The O_2 cathode and Li metal was separated by the single-ion electrolyte. For comparison, the O_2 cathode and Li metal was also separated by the Celgard dipping with 1M LiTFSI TEGDME electrolyte.

ComputationaL Details

Computational Details are given in the Supporting Information.

Results and discussion

Synthesis and characterization of the single-ion electrolyte

MOFs have been previously investigated as for ion conduction of various cations[43] such as proton conductor[44,45] or Li^+ conductor[46-50]. As shown in the **Figure 1a**, Cu-MOF-74 is a nanoporous material comprised of Cu^{2+} metal ion nodes and 2,5-dihydroxyterephthalic acid organic ligands; it has hexagonal, one-dimensional pores lined with Cu^{2+} ions whose open metal sites point directly into the channel. The Cu MOF-74 is carefully chosen from thousands of MOFs because this kind of MOF owns one of the highest open metal site densities known [51] along with suitable electrochemical stability against Li metal. Thus, when the ClO_4^- are coordinated with the open metal center, they will be inside the nanopore of Cu MOF-74.

The Cu MOF-74 was prepared by mixing 4 mmol $Cu(NO_3)_2$ with 2 mmol 2,5- dihydroxyterephthalic acid in the mixed solvent of N,N-Dimethyformamide (DMF) and ethanol; then, after hydrothermal treatment at 80 °C for 12 h, the Cu-MOF-74 is formed. After activating the Cu-MOF-74 at 200 °C under vacuum, the as-obtained activated Cu-MOF-74 is further thermal-treated with 1 M $LiClO_4$ in various solvents (propylene carbonate (PC) for $LiFePO_4$ and $LiMn_2O_4$ full cells, 1,3-dioxolane/ethylene glycol dimethyl ether (DOL/DME(1:1)) for Li||Li symmetric cells, and Tetraglyme (TEGDME) for Li-O_2 batteries) at 80 °C for 12 h in a sealed vessel. Eventually, the

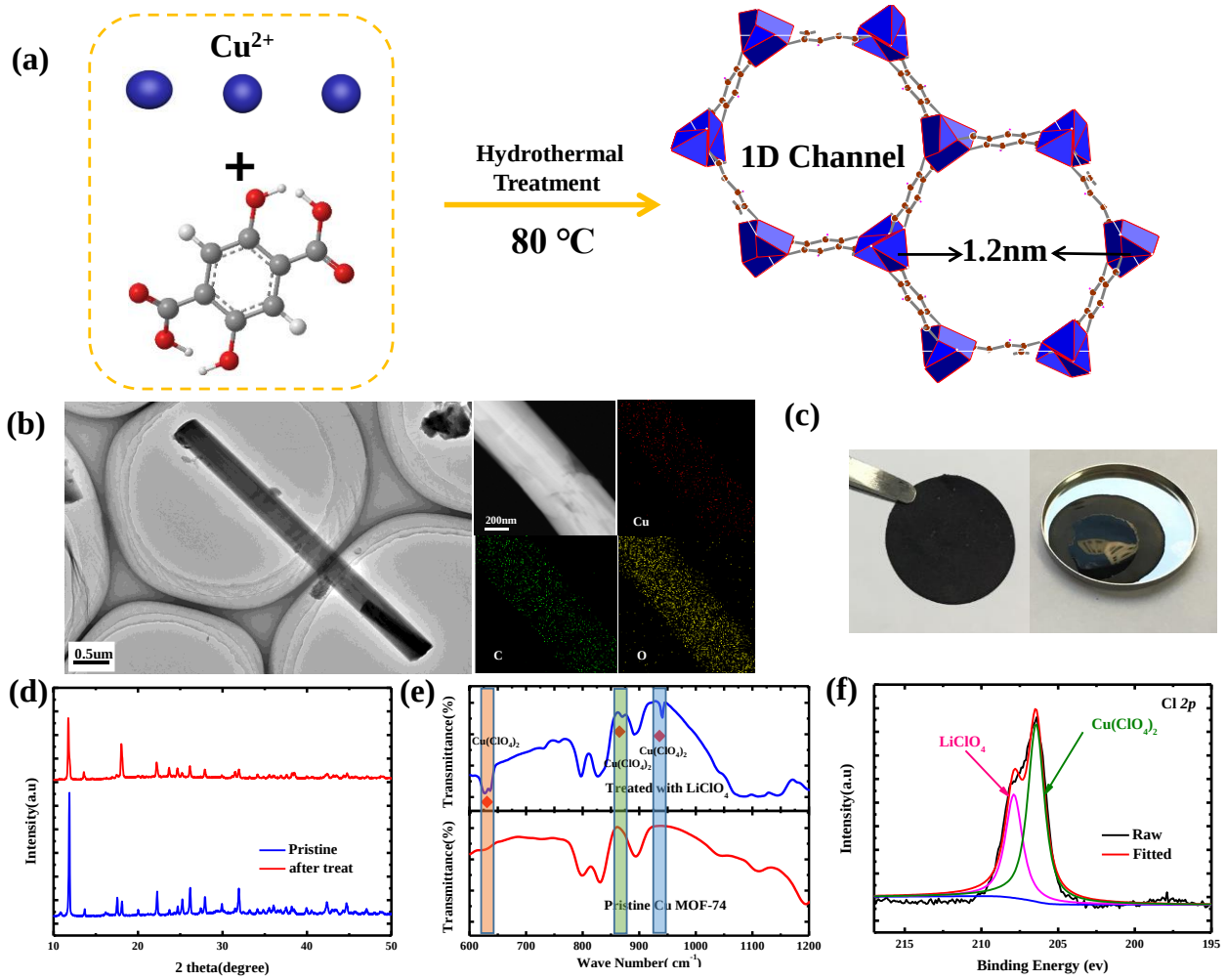

Figure 1. Synthesis and Characterization of the Single-ion electrolyte: a) schematic illustration of the structure of Cu-MOF-74; b) TEM image and corresponding element mapping of Cu-MOF-74; c) Photograph of single-ion electrolyte; d) XRD pattern of Cu-MOF-74 and the single-ion electrolyte; e) FT-IR spectrum of Cu-MOF-74 and Single-ion electrolyte; f) XPS spectrum of Cl *2p* 1/2.

single-ion electrolyte is formed. The as-obtained powders were then compacted under 20 tons of pressure to remove the interparticle pores, and finally the pellet was dried for 30 min at 40 °C under vacuum to remove the excissive solvent.

To investigate the morphology and the composition of the Cu-MOF-74, transmission electron microscope (TEM) was carried out. **Figure 1b** exhibits the TEM image of the Cu-MOF-74, which shows a rodlike morphology, and the element mapping of the Cu-MOF-74 confirms that Cu, C, O elements are uniformly distributed in the MOF particles, which is in accordance with EDS mapping in SEM (**Figure S1**). To further investigate the morphology of Cu-MOF-74, Scanning electron microscopic (SEM) was also carried out. It can be identified in the SEM images that the cross section of Cu-MOF-74 shows a morphology of hexagon. (**Figure S1**)

Figure 1c exhibits the photographs of the single-ion electrolyte. When the liquid electrolyte ($LiClO_4$ in solvent) is dripped on the surface of the compacted single-ion electrolyte, the liquid electrolyte does not permeate into the single-ion electrolyte, indicating that most interparticle voids of the electrolyte have been squeezed out after the compaction process. Further evidence of SEM images of electrolyte sheet (**Figure S2**) also confirm that no obvious piled pores are observed on the surface of the electrolyte, suggesting that the MOF particles of the electrolyte are densely stacked. Further investigation by the EDS mapping equipped in the SEM suggests that C, O, Cu, Cl and F are uniformly distributed in the electrolyte sheet (the F element observed in the electrolyte sheet arises from the PTFE binder). The SEM images of single-ion electrolyte after cycling for 50 times is also given in **Figure S3,** the result suggests the morphology of the single-ion electrolyte remain unchanged.

To further investigate the structure of the single-ion electrolyte, X-ray Diffraction (XRD) is also carried out on the Cu-MOF-74 before and after treating with $LiClO_4$ solution(**Figure 1d**). The XRD pattern of pristine Cu-MOF-74 is finely consistent with the previous published XRD pattern of Cu-MOF-74[52], comfirming that we successfully synthesized the Cu-MOF-74. After treating with $LiClO_4$ solution, the XRD pattern of the Cu-MOF-74 remains unchanged, indicating the structural stability of the Cu-MOF-74 after reaction with $LiClO_4$. The XRD patterns of the single-ion electrolyte after compaction(**Figure S4**) and after cycling for 50 times (**Figure S5**) suggest that the structures of the single-ion electrolyte are stable during the compaction process and cycling.

The reaction between $LiClO_4$ and Cu-MOF-74 was investigated by Fourier transform infrared spectrum (FT-IR) and X-ray photoelectron spectroscopy (XPS). As shown in **Figure 1e**, after treating with $LiClO_4$, some new peaks (630 cm^{-1}, 870cm^{-1} and 950 cm^{-1}) appear in the Cu-MOF-74; these can be assigned to the Cu $(ClO_4)_2$[48]. We also performed the X-ray photoelectron spectroscopy on the Cu-MOF-74 after treating with $LiClO_4$. The Cl *2p 1/2* (**Figure 1f**) is broad, extending from 204 to 210 cm^{-1}, and is fitted by two peaks, one assigned to the $LiClO_4$ (~208.4 eV) and one assigned to $Cu(ClO_4)_2$ (~207.2 eV)[48] Notably, the peak area assigned to Cu $(ClO_4)_2$ is significantly larger than that of $LiClO_4$, indicating that most of the $LiClO_4$ salts have reacted with the open metal sites of Cu^{2+} in the MOF and eventually converted to Cu $(ClO_4)_2$ after thermal treat at 80 °C. Thus, we conclude that after treating with $LiClO_4$ electrolyte, the ClO_4^- anions in the electrolyte react with the Cu-MOF-74 and are anchored on the open metal site of Cu-MOF-74, leaving free solvated Li^+ ions in the pore of Cu-MOF-74. The specific surface area and pore distribution before and after treating with $LiClO_4$ were also measured by the Brunauer-Emmett-Teller method.(See **Figure S6**) The result shows that after treating with $LiClO_4$, the surface area dereases from 630m^2 g^{-1} to 35 m^2 g^{-1} and pore volume sharply reduces from 0.35cc g^{-1} to0.065cc g-1, indicating that the $LiClO_4$ is incorporated into the pore of Cu MOF-74. We also perform the N_2 adsorption and desorption measurement on the Cu MOF-74-PTFE pellet to study the prosity of the single-ion electrolyte. (See **Figure S7**) The result suggest that even after densification under pressure, some stacked pores still exsits.

Ion conductivity investigation of the single-ion electrolyte

To investigate the ion conductivity of the single-ion electrolyte, Electrochemical Impedance Spectroscopy (EIS) was carried out at various temperature ranging from 298K to 333K. The single-ion electrolyte was sandwiched between two stainless steel pellets in the CR2032. Since the ionic conductivity of MOF based ion conductor is highly depent on the amount of solvent in the electrolyte, we also investigated the influence of solvent on the ion conductivity. To investigate the influence of amount of solvent on the ion conductivity, the electrolyte without vacuum drying was also prepared. **Figure 2a** shows the

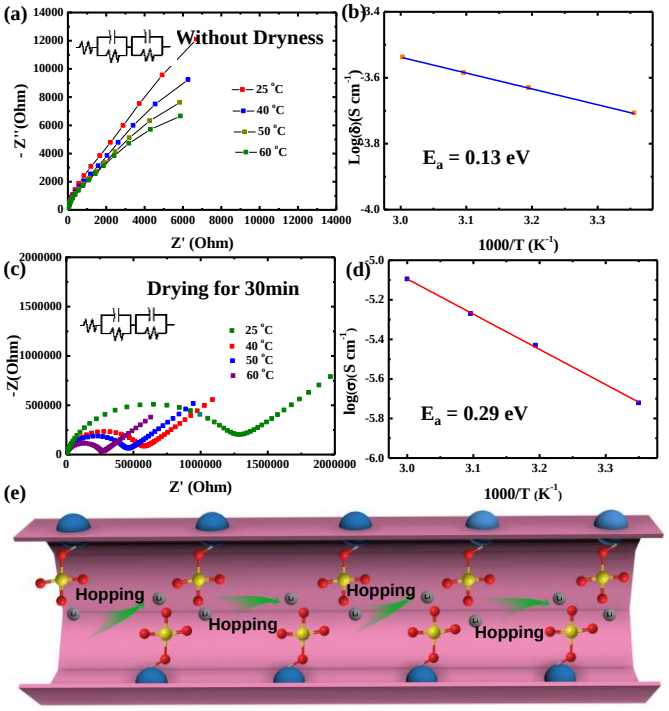

Figure 2. Ion conductivity investigation of the single-ion electrolyte: a) EIS of the electrolyte at various temperatures; b) Arrhenius plot of the single-ion electrolyte; c) Schematic illustration of Li diffusion path in the pore of MOF. (O atom: red, Cl atom: yellow, Cu atom: Blue)

Nyqust plots of the electrolyte at 298K, 313K, 323K and 333K of the electrolyte without vaccum drying. The ion conductivity (S cm^{-1}) was calculated as L/(RS), where L (cm) is the thickness of the electrolyte, R (ohm) is the impedance, and S (cm^2) is the area of the electrolyte. The electrolyte without drying presents a high ion conductivity of 10^{-3} S cm^{-1}. In addition, the electrolyte shows a temperature-dependent conductivity with a typical Arrhenius-like behavior with low activation energy of 0.13 eV. The low activation energy of the single-ion electrolyte suggests that the mechanism of Li^+ transport in the MOF matrix is via a Grotthuss-like mechanism [46]. **Figure 2c** shows the Nyqust plots of the electrolyte at 298K, 313K, 323K and 333K of the electrolyte after drying under vaccum at 40 °C for 30 min. The ion conductivity of the electrolyte after drying reduces to 10^{-5} S cm^{-1} with an activiation energy of 0.29 eV.(**Figure 2d**) Although the activation energy slightly increases after drying under vacuum, it is still below 0.4eV, suggesting that the mechanism of Li^+ transport in the MOF matrix is also via a Grotthuss-like mechanism even with less solvent in the electrolyte. Above all, the results suggest that a higher amount of solvent in the single-ion pellet not only facilitates the ion conductivity of the single-ion pellet but also reduces the activiation energy of ion transport in the single-ion pellet. For comparison, the ion conductivity of the conventional single-ion polymer electrolyte is usually 10^{-7} S cm^{-1} at room temperature. (See **Table S1** for comparison)

Figure 2e schematically illustrates the Li ion transport path in the pore of MOF. Since O containing groups in the MOF are electronegtive and highly lithiophilic[30], the charge is transported by the coordinated hopping of solvated Li^+ between the oxygen groups in the pore of Cu-MOF-74. Hence, we propose two possible pathways for Li ion transport: (a) Li transition between the oxygen sites on Cu-MOF-74 backbone; and (b) Li transition between the perchlorate fragments which are added in the pore of Cu-MOF-74. When the solvated Li ions diffused out of the pore of Cu-MOF-74, they will become free-moving solvated Li ions. However, the free-moving Li-ion prefers to adsorbed into the pore of neighboring Cu-MOF-74, because of the presence of highly lithiophilic and electronegative ClO_4^- inside the pore of Cu-MOF-74.

To confirm the single-ion transport mechanism, Li transference number was also calculated by potentiostatic polarization method on the basis of Bruce- Vincent- Evans equation[53]. (See **Figure S8** for details) The calculated Li ion transference number is as high as 0.82, indicating that most of the anion are immobilized on the open metal site. However, the typical Li transference number in the conventional liquid batteries with Celgard separator is only around 0.2-0.442.[34,48]

To further probe the electrochemical window of the single-ion electrolyte, Cyclic Voltammetry (CV) were also carried out with a scan rate of 1 mV s^{-1} from -0.2V – 5.0V. The electrochemical window of the single-ion electrolyte is from 2.1 V- 4.9 V, which makes it appropriate for use with most cathode materials. (See **Figure S9** and the associated discussion). To probe whether the MOF backbones in the single-ion electrolyte paticipate in the formation of solid electrolyte interface(SEI), the XPS spectrum was also carried out on the Li metal which is retracted from the Li||Li symmetric cell.(See **Figure S10** and corresponding discussion) As shown in **Figure S10**, some peaks correponding to carboxyl groups and hydroxyl groups are observed on the surface of Li metal. Since the solvent in Li||Li symmetric cells is DOL/DME, which is stable against Li metal. Those carboxyl group and hydroxyl groups based SEI layer comes from the MOF backbone. In conclusion, the MOF backbones in the single-ion electrolyte participate in the formation of SEI layer on the surface of the Li metal.

Theoretical investigation of the Li^+ transport mechanism in the single-ion electrolyte

Due to their unique structure, MOFs have been widely investigated for proton conduction, [44,45] and two key factors are found to be indispensable for the proton conduction in MOFs. The first factor is a certain degree of humidity, while the second factor is the presence of highly hydrophilic and electronegative functional groups (most commonly $-SO_3^{2-}$) in the nanopore of MOFs. For the proton transport inside the pore of MOF, the most common mechanism is the Grotthuss mechanism where solvated protons hop between two neighboring sulfonate groups inside the pore of MOF matrix. When the protons diffuse out of the nano-pore of the MOF into the void between MOF particles, they will become free-moving hydrated protons between two adjacent MOF particles. However, it is favorable for them to be adsorbed into the pore of the neighboring MOF particles because there are abundant highly hydrophilic and electronegative sulfonate groups in the pore of the MOFs. Hence, the proton conduction in the MOFs are dominated by the proton transport in the pore of the MOF matrix. This mechanism has also been proposed for Li ion conduction in MOFs[46-50]; when the two indispensable components (i.e. the highly lithiophilic groups inside the pores of MOFs and solvent) are present, the MOF can support Li^+ transport in the nanopores. For example, a sulfonate-functionalized MOF separator was previously reported as an ion sieve for separating cations (e.g. H^+, Li^+, Na^+, Mg^{2+}) in water.[46]

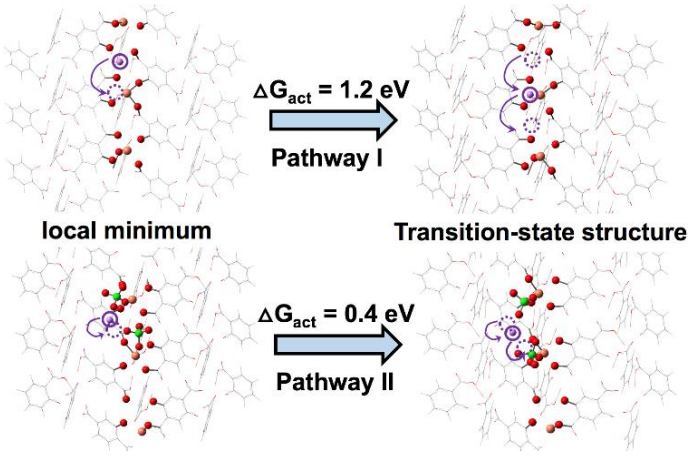

Figure 3. Quantum chemistry investigation of Li migration in the single-ion electrolyte. The MOF backbone is drawn in the wireframe style, and the atoms that are allowed to be relaxed during geometry optimization are explicitly shown (Colour code: Cu orange, O red, C grey, H white, Li violet, and Cl green).

To investigate the Li^+ transport mechanism in the single-ion electrolyte proposed here, quantum chemistry calculations were performed to compute the free energies of activation ΔG_{act} for the two possible pathways mentioned above. For this purpose, we first optimized the bulk structure of Cu-MOF-74 by spin-polarized Kohn-Sham density functional theory (DFT) with the PBE-D3(BJ) exchange-correlation functional and periodic boundary conditions. We then carved a cluster model with the formula $C_{181}H_{87}Cu_{24}O_{94}$ from the periodic-DFT optimized bulk structure, and free energies of activation were computed by finite-cluster calculations in the presence of a solvent reaction field with the solvent modeled as diethyl ether. The DFT-optimized crystalline structure of Cu-MOF-74 is shown in **Figure S11**, and the cluster model is shown in **Figure S12**.

Figure 3 depicts the two possible migration pathways, with the MOF backbone drawn in wireframe style and the atoms that are allowed to relax during the cluster geometry optimization shown explicitly. To simulate the Li transport process in batteries, the Gibbs free energy barriers are corrected with self-consistent reaction filed (SCRF) calculations in diethyl ether (DME) solvent. The first path is Li^+ hopping between the O hollow sites on Cu-MOF-74 matrix (**Path I**), while the second path is Li^+ hopping between the ClO_4^- anchored on the open metal site of Cu-MOF-74 (**Path II**). The Gibbs free energies of activation were computed at 298 K for these two possible pathways. As shown in **Figure 3**, ΔG_{act} for Li^+ hopping between oxygen hollow sites (**Path I**) on Cu-MOF-74 is about 1.2 eV, and ΔG_{act} for Li^+ hopping between perchlorate fragments (**Path II**) in Cu-MOF-74 is only about 0.4 eV. Considering the lower migration energy barrier of Path II compared with Path I, we conclude that Li^+ migration in the single-ion electrolyte is dominated by the hopping of Li ion between the ClO_4^- anchored on the open metal site of Cu-MOF-74. As a result, homogeneous Li ion flux is achieved by the single-ion electrolyte.

Morphology of the Li metal with single-ion electrolyte

The surface morphology of the Li metal in the different electrolyte was investigated by the ex-situ SEM. The Li||Li symmetric batteries were assembled with different electrolyte and then cycled for a certain period of time. **Figure 4** shows the morphology of the Li metal in different electrolyte and obvious differences are evident on the morphology of Li metal cycling in different electrolyte. The Li||Li symmetric batteries with LiClO4 DOL/DME can only cycle for 10 h, and the SEM images of Li metal after cycling for 10h with $LiClO_4$ DOL/DME electrolyte presents a rough surface with loosely stacked deposits. These loosely stacked Li metals are especially vulnerable to the attack of electrolyte and can be easily peeled off from the Li metal. When employing LiTFSI DOL/DME, the cycle life prolonged over 100h. The SEM images of the Li metal also shows a loose and rough surface with obvious needle-like Li dendrites coating on the surface of Li metal. While a compact and smooth surface are observed on Li cycling with the single-ion electrolyte even after 100 h. Above all, a smooth surface with compact stack of Li is achieved with the single-ion electrolyte.

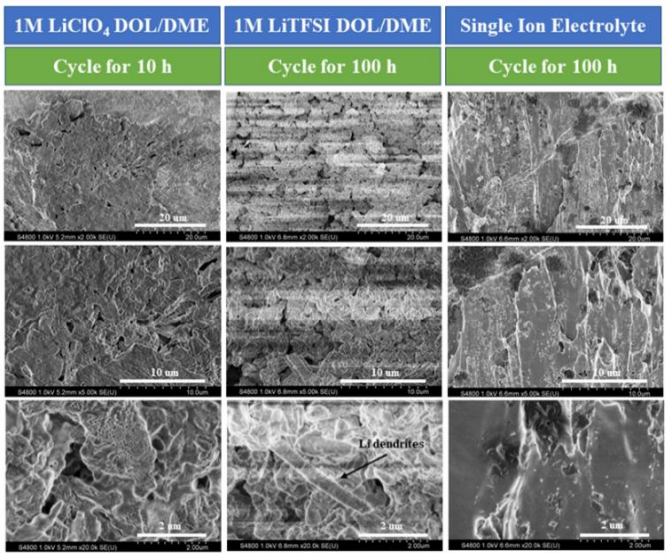

Figure 4. Morphology of Li metal with different electrolyte.

Electrochemical performance of Li||Li symmetric batteries and Li||$LiFePO_4$ full cells with single-ion electrolyte

To investigate the electrochemical performance of the single-ion electrolyte, Li||Li symmetric cells were assembled by separating two pieces of Li metal by the single-ion electrolyte. As shown in the **Figure 5a**, the Li||Li symmetric cell exhibits an ultralong cycle life over 2000 h without short circuits at the current density of 0.2 mA cm^{-2}, indicating the superior ability of the single-ion electrolyte to suppress the Li dendrite. In addition, the Li||Li symmetric cell with single-ion electrolyte shows a low voltage hysteresis of 40 mV for the first several cycles, which reduces to 20 mV after 400 h and then remains 20 mV over 2000 h. Even after 2000 h, no sign of short circuits is observed for the Li||Li symmetric cells with the single-ion electrolyte. When the Li||Li symmetric cells are tested at higher current density with higher deposition capacity, excellent performance is also achieved (**Figure S13**). For comparison, the Li||Li symmetric cell was also assembled with Celgard infiltrated in LiTFSI DOL/DME electrolyte, which is cycled at low current rate of 0.2mA cm^{-2}., the polarization suddenly increased only after 400 h (**Figure S14**). To our knowledge, the cycle life of Li||Li symmetric batteries with our single-ion electrolyte is the best ever reported.(See **Table S2** for comparison)

To further investigate the property of the single-ion electrolyte, Li||$LiFePO_4$ full cells were also assembled in the glovebox. As shown in the **Figure 5b**, the Li||$LiFePO_4$ full cell shows a specific capacity of 163 mAh g^{-1} at the rate of 0.2C (1C = 170 mAh g^{-1}), which slightly reduces to 160m Ah g^{-1} at the rate of 0.5C. when the current density increases to 1C, a specific capacity of 150 mAh g^{-1} is also achieved. In addition, when the current density further increases to 2C and 5C, high capacity of 140 mAh g^{-1} and 110 mAh g^{-1} are also achieved with the single-ion electrolyte. The corresponding voltage profiles at different current density are presented in the **Figure 5c**. It can be identified that even at high current rate of 5C, the polarization of the full cell is only 0.4V.

Figure 5d shows the cycle performance of Li||$LiFePO_4$ full cells with the single-ion electrolyte at the rate of 1C. It is identified that the cell with the single-ion electrolyte present an

initial discharge capacity of 142 mAh g^{-1}, which slightly increases to 151mAh g^{-1} after 10 times. The specific capacity of Li||$LiFePO_4$ full cell maintains over 150 mAh g^{-1} without any decay after 200 times. Then, the specific capacity slightly decreases to 142 mAh g^{-1} after 300 cycles, and 138 mAh g^{-1} after 500 cycles, which corresponds a capacity retention of 100% and 97.2% of the initial capacity respectively. Even after 2000 cycles, a specific capacity of 106.5 mAh g^{-1} is also achieved for the single-ion electrolyte, corresponding to capacity retention of over 75%. To our knowledge, it is the longest cycle life ever reported in the Li||$LiFePO_4$ full cells (See **Table S3** for comparison). For comparison, the cycle stability of Li||$LiFePO_4$ full cell was also investigated in the conventional electrolyte, which exhibits inferior cycle life. **Figure 5e** presents the corresponding voltage curves of Li||$LiFePO_4$ with the single-ion electrolyte at rate of 1C. It can be identified that the overpotential of the Li||$LiFePO_4$ remains almost unchanged for the first 500 cycles. Even after 2000 cycles, the overpotential is only slightly increased. However, the polarization of Li||$LiFePO_4$ full cells with conventional liquid electrolyte became severer only after 100 cycles (**Figure S15**). The cycle performance of Li||$LiFePO_4$ full cell and the corresponding voltage profiles of Li||$LiFePO_4$ full cells at 0.2C and 0.5C were also presented in the Supporting Information as **Figure S16** and **Figure S17**, which also exhibits excellent cycle performance.

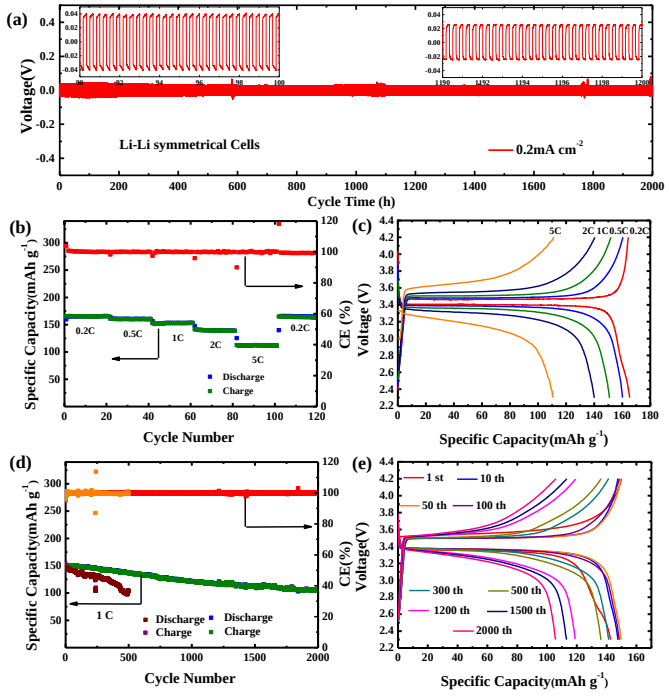

Figure 5. Electrochemical performance of Li-metal batteries with single-ion electrolyte: a) Li||Li symmetric cell with single-ion electrolyte at a current density of 0.2 mA cm^{-2}; b) rate performance of Li||$LiFePO_4$ full cell with single-ion electrolyte; c) corresponding voltage profile of Li||$LiFePO_4$; d) Cycling performance of Li||$LiFePO_4$ full cells with single-ion electrolyte at the rate of 1C; e) Corresponding voltage profiles of single-ion electrolyte at 1C during cycles.

Electrochemical performance of Li||$LiMn_2O_4$ full cells with Single-ion electrolyte

$LiMn_2O_4$ with the spinel structure is a very promising cathode for the Li batteries owing to the high specific capacity, high operating voltage of 4V, low cost, superior safety and long cycle life within a wide working temperature range[54]. However, the poor cycling performance of this material, in particular at elevated temperatures, limits its wide application as a cathode material for Li metal batteries[54]. Previous report[54] has shown that the capacity fade of 4 V $LiMn_2O_4$ cells is directly associated with the dissolution of Mn^{2+} from the cathode/electrolyte interface because of the disproportionation reaction of Mn (III), and the subsequent deposition of Mn^{2+} on the anode. Herein, we show that our single-ion electrolyte can effectively suppress the dissolution of Mn^{2+} into the electrolyte and thus improve the cycle stability of $LiMn_2O_4$||Li full cell.

Figure 6a shows the cycling performance of $LiMn_2O_4$||Li full cell at room temperature. It is identified in **Figure 6a**, the $LiMn_2O_4$||Li full cell exhibits initial discharge capacity of 116mAh g^{-1}. After 250 cycles a discharge capacity of 106mAh g^{-1} is still achieved, corresponding to a capacity retention of 92.2%. For comparison, the cycling performance Li||$LiMn_2O_4$ full cell in the traditional liquid electrolyte only shows a capacity retention of 83%. The corresponding voltage profiles over cycles are given in **Figure 6b**. For comparison. the corresponding voltage curve of Li||$LiMn_2O_4$ full cells in the conventional electrolyte is given in **Figure S18a**. When the working temperature increases to 55^oC, the comparison of the capacity retention becomes much more obvious. **Figure 6c** shows the cycling performance of $LiMn_2O_4$||Li full cells at 55 ^oC. It can be noted that the $LiMn_2O_4$||Li full cell exhibits an initial discharge capacity of 114mAh g^{-1}, which reduces to 81.3 mAh g^{-1} after 250 cycles with single-ion electrolyte, corresponding to a capacity retention of 72% after 250 cycles at 55°C. However, the capacity retention is only 52% with conventional liquid electrolyt e after 250 cycles. **Figure 6d** shows the corresponding voltage curves of $LiMn_2O_4$||Li full cell with single-ion electrolyte. The corresponding voltage curves with conventional electrolyte at 55 ^oC are also given in **Figure S18b**.

Previous report[55] has shown that the dissolution of Mn^{2+} in the $LiMn_2O_4$ batteries involves in a series of processes including the dissolution of Mn^{2+} into the electrolyte, and then the

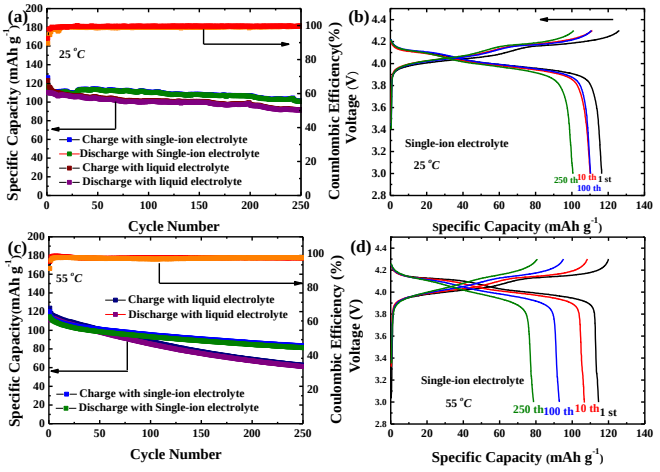

Figure 6. Li||$LiMn_2O_4$ full cells at the rate of 1C: a) Cycling performance at the rate of 1C at room temperature; b) Corresponding voltage profiles of the cell with single-ion electrolyte at room temperature; c) Cycling performance at the rate of 1C at 55 ^oC; d) Corresponding voltage profiles of single-ion electrolyte at 55 ^oC.

migration of Mn^{2+} from cathode region to the anode region. Eventually, the Mn^{2+} will deposit on the surface of the anode. This process will result in the structural change of $LiMn_2O_4$ cathode, which is responsible for the capacity decay of the $LiMn_2O_4$||Li batteries. Since the ion diameter of Mn^{2+} is significantly larger than that of Li ion, the migration rate of Mn^{2+} inside the pore of Cu MOF-74 is much slower than that of Li^+. As a result, this single-ion electrolyte can suppress the dissolution of Mn^{2+}. Thus, improved cycle stability is achieved for $LiMn_2O_4$||Li full cells with the single-ion electrolyte even at elevated temperature.

Electrochemical performance of Li-O_2 batteries with single-ion electrolyte

To further demonstrate the application of the single-ion electrolyte, Li-O_2 batteries was also assembled with single-ion electrolyte. **Figure 7a** schematically illustrates the structure of the Li-O_2 cells. The cathode was prepared by mixing 90wt% Kejenblack and 10 wt% PVDF. Then, CR2036 Li-O_2 coin cells were assembled by separating the cathode and Li metal with single-ion electrolyte. **Figure 7b** exhibits the midpoint voltage of the Li-O_2 batteries with single-ion electrolyte and traditional G4 electrolyte. It can be identified that the polarization of the Li-O_2 cell with single-ion electrolyte is much lower than that of Li-O_2 batteries with G4 (1M LiTFSI in TEGDME) electrolyte. The decrease in the polarization may be attributed to the catalytic activity of MOF-74 for Li peroxide, which has been demonstrated by the previous reports [56,57]. **Figure 7c** shows the voltage profiles of Li-O_2 cell with G4 electrolyte. Only after 40 cycles, the cut-off discharge voltage drops below 2.0V. while the cycle life of Li-O_2 cells with single-ion electrolyte (**Figure 7d**) further prolonged to 50 times with lower polarization. Even after 50 cycles, the cut-off discharge voltages of Li-O_2 cells is still above 2.0V. It should be noted that the cycle life of Li-O_2 batteries may be limited by the KB cathode, as the lithium peroxides formed during discharge may clog the pore of KB, leading to the decay of batteries. Above all, an improved performance of Li-O_2 batteries is achieved by the single-ion electrolyte.

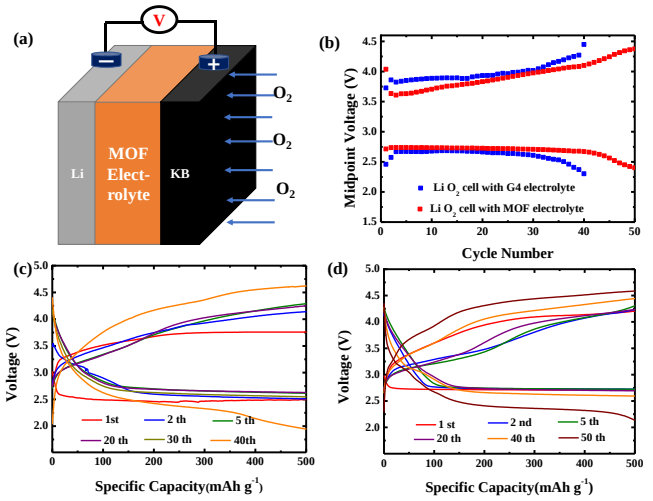

Figure 7. Performance of Li-O_2 cells with single-ion electrolyte: a) Schematically illustration of Li-O_2 Cell structure with single-ion electrolyte; b) comparison of mid-point voltage of Li-O_2 cells with single-ion electrolyte (Red) and traditional G4 electrolyte (Blue); c) Voltage profiles of Li-O_2 batteries with G4 electrolyte; d) Voltage profiles of Li-O_2 batteries with single-ion electrolyte.

Conclusions

We report a versatile single-ion electrolyte, which is achieved by coordinating the anion on the open metal site of Cu-MOF-74. The single-ion electrolyte prepared in this way radically changes the behavior of Li^+ migration in the electrolyte, which opens a new pathway departure from the traditional solid electrolyte or polymer electrolyte to realize homogeneous single-ion transport in the liquid electrolyte. When the electrolyte is assembled into $LiFePO_4$-Li metal batteries, the Li dendrites are suppressed. As a result, an ultralong cycle life of 2000 times with a capacity retention of nearly 75% is achieved for Li||$LiFePO_4$ full cells with this single-ion electrolyte. When the single-ion electrolyte is applied for $LiMn_2O_4$||Li batteries, the dissolution of Mn^{2+} is suppressed and an improved performance is achieved even at high temperature. Finally, when the single-ion electrolyte is employed as the electrolyte for Li-O_2 batteries, an improved cycle life with reduced overpotential is also achieved.

Conflicts of interest

There are no conflicts to declare.

Author's Contribution

Shouyi Yuan conceived this idea and designed the experiments. Junwei Lucas Bao carried out the theoretical calculations. Jishi Wei helped to plot the 3D max scheme in Figure 2e. Yonggang Wang, Yongyao Xia and Donald G. Truhlar directed the project. Shouyi Yuan performed the material synthesis, characterization, electrochemical measurements and data analysis. Shouyi Yuan, Junwei Lucas Bao and Donald G. Truhlar co-wrote the paper. All authors discussed the results and commented on the manuscript.

Acknowledgements

We acknowledge funding from the National Natural Science Foundation of China (21622303), the State Key Basic Research Program of China (2016YFA0203302), and the U.S. Department of Energy, Office of Basic Energy Sciences (DE-FG02-17ER16362).

Notes and references

1 M. Armand and J. M. Tarascon, *Nature* 2008, **451**, 652–657.
2 X.B. Cheng, R. Zhang, Z.C. Zhao and Q. Zhang, *Chem. Rev.* 2017, **117**, 10403-10473.
3 W. Xu, J.L. Wang, F. Ding, X.L. Chen, E. Nasybulin, Y.H. Zhang, and J.G. Zhang, *Energy Environ. Sci.* 2014, **7**, 512-537.
4 R. Zhang, N.W. Li, X.B. Cheng, Y.X. Yin, Q. Zhang and Y.G. Guo, *Adv. Sci.* 2017, **4**, 1600445.
5 S.Y. Yuan, J.W.L. Bao, L.N. Wang, Y.Y. Xia, D. G. Truhlar and Y.G. Wang, *Adv. Energy.Mater.* 2016, **6**, 1501733.

6 J. Zhang, C.P. Yang, Y.X. Yin, L.J. Wan and Y.G. Guo, *Adv. Mater.* 2016, **28**, 9539-9544.
7 G.Y. Xu, B. Ding, P. Nie, L.F. Shen, H. Dou and X.G. Zhang, *ACS Appl. Mater. Inter.* 2014, **6**, 194-199.
8 F. Li, Y. Chen, D.M. Tang, Z. Jian, C. Liu, D. Golberg, A. Yamadad and H. Zhou, *Energy Environ. Sci.* 2014, **7**, 1648-1652.
9 X.G. Yang, J.J. Xu, Z.W. Chang, D. Bao, Y.B. Yin, T. Liu, J.M. Yan, D.P. Liu, Y. Zhang and X.B. Zhang, *Adv. Energy Mater.* 2018, **8**,1702242.
10 Y.N. Chen, Q. Zhang, Z. Zhang, X.L. Zhou, XL Y.R. Zhong, M. Yang, Z.J. Xie, J.P. Wei and Z. Zhou, *J. Mater. Chem. A*, 2015, **3**, 17874-17879.
11 N. Chen, Y.J. Dai, Y. Xing, L. Wang, C. Guo, R. J. Chen, S.J. Guo and F. Wu, *Energy Environ. Sci.* 2018, **9**, 1803372.
12 S.H. Jiao, X.D. Ren, R.G. Cao, M.H. Engelhard, Y.Z. Liu, D.H. Hu, D.H. Mei, J.M. Zheng, W.G. Zhao, Q.Y. Li, N. Liu, B.D. Adams, C. Ma, J. Liu, J.G. Zhang and W. Xu, *Nat. Energy,* 2018, **3***,* 739-746.
13 X.L. Fan, L. Chen, O. Borodin, X. Ji, J. Chen, S. Hou, T. Deng, J. Zheng, C.Y.Yang, S.C. Liou, K. Amine, K. Xu, and C.S. Wang, *Nat. Nano.* 2018, **13**, 715-722.
14 L.M. Suo, Y.S. Hu, H. Li, M. Armand and L.Q. Chen, *Nat. Commun.* 2013, **4**, 1481.
15 C. Yan, X.Y. Yao, X. Chen, X.B. Chen, X.Q. Zhang, J.Q. Huang and Q. Zhang, *Angew. Chem. Int. Ed.* 2018, **57**, 1807034.
16 Q. Pang, X. Liang, A. Shyamsunder and L.F. Nazar, *Joule* 2017, **1**, 871-886.
17 J.M. Zheng, P.F. Yan, D.H. Mei, M.H. Engelhard, S.S. Cartmell, B. J. Polzin, C.M. Wang, J.G. Zhang and W. Xu, *Adv. Energy Mater.* 2016, **6**, 1502151.
18 F. Chu, J. Hu, C. Wu, Z. Yao, J. Tian, Z. Li and C. Li, *ACS Appl. Mater. Inter.* 2019, **11**, 3869-3879.
19 B. Zhou, L. Guo, Y. Zhang, J. Wang, L. Ma, W. Zhang, Z. Fu and Z. Peng, *Adv. Mater.* 2017, **29**,1701568.
20 X. Liang, Q. Pang, I.R. Kochetkov, M.S. Sempere, H. Huang, X. Sun and L.F. Nazar, *Nat. Energy,* 2017, **2**, 17119.
21 J. Hu, K.Y. Chen and C. Li, *ACS Appl. Mater. Inter.* 2018**, 10**, 34322-34331.
22 B. Zheng, J. Zhu, H. Wang, M. Feng, E. Umeshbabu, Y. Li, Q. Wu and Y. Yang, *ACS Appl. Mater. Inter.* 2018, **10**, 25473-25482.
23 J. Yan, J. Yu and B. Ding, *Adv. Mater*. 2018, **30**, 1705105.
24 H. Zhao, D. Lei, Y. He, Y. Yuan, Q. Yun, B. Ni, W. Lv, B. Li, Q. Yang, F. Kang and J. Lu, *Adv. Energy. Mater.* 2018, **8**, 1800226.
25 L. Lu, J. Ge, J. Yang, S. Chen, H.B. Yao, F.Zhou and S.H.Yu, *Nano Lett.* 2016, **16**, 4431;
26 D.C. Lin, J. Zhao, J. Sun, H.B.Yao, Y.Y. Liu, K. Yan and Y. Cui, *Proc. Natl. Acad, Sci.* 2017, **114**, 4613–4618;
27 S. Liu, A.X. Wang, Q. Li, J.S. Wu, K.V. Chiou, J.X. Huang and J.Y. Luo, *Joule*, 2018, **2,** 184-193.
28 W.D. Zhang, H.L.L. Zhuang, L. Fan, L.N. Gao, and Y.Y. Lu, *Sci. Adv.* 2018**, 4**, eaar4410.
29 D. Zhou, R.L. Liu, Y. He, F. Li, M. Liu, B. Li, Q. Yang, Q. Cai and F. Kang, *Adv. Energy Mater.* 2016, **6**,1502214.
30 S. Yuan, J.L. Bao, C. Li, Y. Xia, D.G. Truhlar and Y. Wang, *ACS Appl. Mater. Inter.* 2019, **11**, 10616-10623
31 W.Liu, Y.Mi, Z.Weng, Y.Zhong, Z.Wu and H. Wang, *Chem. Sci.* 2017, **8**, 4285-4291.
32 B.Q. Li, X.R. Chen, X. Chen, C.X, Zhao, R. Zhang, X.B. Cheng and Q. Zhang, *Research*, 2019, **2**, 4608940.
33 H. Zhang, C.M. Li, M. Piszcz, E. Coya,T. Rojo, L.M. Rodriguez-Martinez, M. Armand and Z.B. Zhou, *Chem. Soc. Rev.* 2017, **46,** 797-815.
34 C.C. Li B.S. Qin, Y.F. Zhang, A. Varzi, S. Passerini, J.Y. Wang, J.M. Dong, D.L. Zeng, Z.H. Liu and H.S. Cheng, *Adv. Energy Mater.* 2019, **9**, 1803422.
35 C. Yang, K. Fu, Y. Zhang, E. Hitz and L.B Hu, *Adv. Mater.* 2017 **29**, 1701169
36 Z. Wang, Z. Wang, L. Yang, H. Wang, Y. Song, L. Han, K. Yang, J. Hu, H. Chen and F. Pan, *Nano Energy*, 2018, **49**, 580-587.
37 X. Yan, Z. Li, Z. Wen, and W. Han, *J. Phys. Chem. C*, 2017, **121**, 1431-1435.
38 K.E. Thomas,S.E. Sloop, J.B. Kerr and J. Newman, *J. Power Sources* 2000, **89**, 132–138.
39 M. D. Tikekar, Lynden A. Archer and D. L. Koch, *Sci. Adv.* 2016, **2**, e1600320.
40 Y. Lu, M.D. Tikekar, R. Mohanty, K. Hendrickson, L. Ma and L.A. Archer, *Adv. Energy Mater.* 2015, **5**, 1402073.
41 M.D. Tikekar, L.A. Archer and D.L. Koch, *J. Electrochem. Soc.* 2014, **161,** A847-A855.
42 S. Bai, Y. Sun, J. Yi, Y. He, Y. Qiao and H. Zhou, *Joule*, 2018, **2**, 2117-2132.
43 S. Horike, D. Umeyama and S.I. Kitagawa, *Acc. Chem. Res.* 2013, **46**, 2376-2384.
44 F. Yang, G. Xu, Y. Dou, B. Wang, H. Zhang, H. Wu, W. Zhou, J. Li and B. Chen, *Nat. Energy*, 2017, **2,** 877-883.
45 Y. Guo, Z.Q. Jiang, W. Ying, L.P. Chen, Y.Z. Liu, X.B. Wang, Z.J. Jiang, B.L. Chen and X.B. Peng, *Adv. Mater.* 2017, **30***,* 1705155.
46 Y. Guo, Y.L. Ying, Y.Y. Mao, X.S. Peng and B.L. Chen, *Angew. Chem. Int. Ed.* 2016, **55**, 15120-15124.
47 Z. Wang, R. Tan, H. Wang, L. Yang, J. Hu, H. Chen and F. Pan, *Adv. Mater.* 2018, **30**, 1704436
48 L. Shen, H.B. Wu, F. Liu, J.L. Brosmer, G.R. Shen, X.F.Wang, J.I. Zink, Q.F. Xiao, M. Cai, G. Wang, Y.F. Lu and B. Dunn, *Adv. Mater.* 2018**, 30**, 1707476.
49 S.S. Park, Y. Tulchinsky and M. Dinca, *J. Am. Chem. Soc.* 2017, **139**, 13260-13263.
50 B.M. Wiers, M.L. Foo, N.P. Balsara and J.F. Long, *J. Am. Chem. Soc*. 2011**, 133***,* 14522-14525.
51 E. Haldoupis, J. Borycz, H.L. Shi, K.D. Vogiatzis, P. Bai, W.L. Queen, WL L. Gagliardi and J.I. Siepmann, *J. Phys. Chem. C* 2015, **119***,* 16058-16071.
52 Y.J. Liao, L. Zhang, M.H. Weston, W. Morris, J.T. Hupp and O.K. Farha, *Chem. Commun.* 2017, **53**, 9376-9379.
53 J. Evans, C.A.Vincent and P.G. Bruce, *Polymer* 1987, **28**, 2324-2328.
54 J. Lu, C. Zhan, T.P. Wu, J.G. Wen, Y. Lei, A.J. Kropf, H.M. Wu, D.J. Miller, J.W. Elam, Y.K. Sun, X.P. Qiu and K. Amine, *Nat. Commun.* 2014, **5**, 5693.
55 C. Zhan, T. Wu, J. Lu and K.Amine, *Energy Environ. Sci.* 2018, **11**, 243-257.
56 W.J. Yan, Z.Y. Guo, H.S. Xu, Y.B. Lou, J.X. Chen and Q.W. Li, *Mater. Chem. Front.* 2017, **1,** 1324-1330.
57 D.F. Wu, Z.Y. Guo, X.B. Yin, Q.Q. Pang, B.B. Tu, L.J. Zhang, Y.G. Wang and Q.W. Li, *Adv. Mater,* 2014, **26**, 3258-3262.

Broad Context

Given the limitations inherent in current battery technologies, much of the research on next generation energy storage technologies has been focused on potential successors to lithium ion batteries such as Li-S batteries or Li-O_2 batteries. However, the use of alkali metal anodes is needed to realize the potential of these batteries, but these anodes are likely to suffer from dendrite formation that results in excessive electrolyte decomposition. In this work, we present a versatile single-ion electrolyte, which is achieved by a different strategy of coordinating the anions in the electrolyte on the open metal site of metal organic framework. Further theoretical calculations suggest that the Li ion transport in this electrolyte is via a Grotthuss-like mechanism involving hopping of Li ion between ClO_4^-. The single-ion electrolyte is versatile, which has wide applications including suppressing the Li dendrites, suppressing the dissolution of the Mn^{2+} in Li||$LiMn_2O_4$ full cells and reducing the polarization of Li-O_2 batteries. As a result, improved performances are achieved for all the batteries.